Dissociative photoionization of H_2 and D_2 by (30–37)-eV photons via $^1\Pi_u$ states

I. Sánchez and F. Martín
Departamento de Química C-9, Universidad Autónoma de Madrid, 28049 Madrid, Spain
(Received 25 March 1999)

We present a theoretical study of dissociative photoionization of H_2 and D_2 via $^1\Pi_u$ states, in the photon energy range 30–37 eV where several ionization and dissociation channels are open. The theory includes coherently competition between the different dissociation and ionization channels, and makes use of *B*-spline functions to represent both the electronic and nuclear motions. Our results agree fairly well with recent experiments, and show that the various peaks observed in the spectra are due to the lowest Q_2 $^1\Pi_u$ doubly excited state, which decays following both a direct and a multistep mechanism. The differences between H_2 and D_2 results can be explained in terms of calculated Franck-Condon factors and autoionization probabilities. [S1050-2947(99)10109-4]

PACS number(s): 33.80.Eh, 33.80.Gj

I. INTRODUCTION

Molecular photoionization is currently used to probe electronic and vibrational continua of simple diatomic molecules. In the case of H_2, absorption of photons with energy $\hbar\omega > 18.1$ eV leads to emission of an electron and dissociation of the molecule according to the equation $H_2 + \hbar\omega \rightarrow H + H^+ + e^-$. The latter process is called dissociative photoionization, and plays a fundamental role in interstellar clouds, planetary atmospheres, and plasma physics. The first investigations of dissociative ionization were performed in the early 1970s by analyzing the kinetic-energy distribution (KED) of the resulting protons [1–8], and its angular dependence [9]. Experimental evidence of resonance effects was obtained by Strathdee and Browning [10], who observed a significant enhancement of the proton production rates at 26.9 and 30.5 eV. This enhancement was immediately related to the existence of doubly excited states in H_2 [10–13], in particular the lowest $^1\Sigma_u^+$ state, which belongs to the Q_1 resonance series converging to the $^2\Sigma_u^+(2p\sigma_u)$ ionization threshold (see Fig. 1). Subsequent experimental works in this energy region [14–19] revealed additional features that the theory has not been able to explain until very recently [20,21].

At higher photon energies ($\hbar\omega > 30$ eV) the situation is more complicated because several ionization channels are open (see Fig. 1). Furthermore, doubly excited states lying above the $^2\Sigma_u^+(2p\sigma_u)$ threshold (the so-called Q_2 states) are also accessible, and may autoionize, yielding H_2^+ in either the $^2\Sigma_g^+(1s\sigma_g)$ or $^2\Sigma_u^+(2p\sigma_u)$ states. This energy region was explored in two recent experiments by Ito, Hall and Ukai [17] and Latimer *et al* [22], who determined the kinetic-energy distribution of ejected protons and deuterons in H_2 and D_2, respectively. Although the experiments are rather contradictory (the former authors found some resonance peaks that are absent in the spectra of Ref. [22]), they both showed a strong isotope effect which results in a significant increase of the D^+ yield, especially at the higher kinetic energies. In a recent paper [23], we reported *ab initio* calculations of KED spectra for H_2 in the energy range 30–37 eV, and for protons observed at 90° with respect to the polarization vector of the incident radiation. For this observation angle, only the $^1\Pi_u$ continuum is populated [9]. We have shown that multichannel dissociation through a single $^1\Pi_u$ doubly excited state leads to multifeatured spectra similar to those reported by Ito, Hall and Ukai [17]; the different peaks observed in each dissociation channel have been interpreted in terms of a direct and a multistep mechanism. In the present paper we present additional results for D_2, and analyze the origin of the isotope effect reported in the experiments. These results will allow us to discuss in more detail the validity of the conclusions reported in Ref. [23].

The paper is organized as follows. In Sec. II we describe the theoretical method and its implementation with *B*-spline functions. The results for H_2 and D_2 are presented and discussed in Sec. III. Finally, some conclusions are summarized in Sec. IV. Atomic units are used throughout unless otherwise stated.

II. THEORY

The theoretical method, inspired in the ideas of Refs. [24] and [25], is a generalization of the one used in Refs. [20,21] for the special case of a single ionization channel. It makes use of *B*-spline functions [26] to represent both the electronic

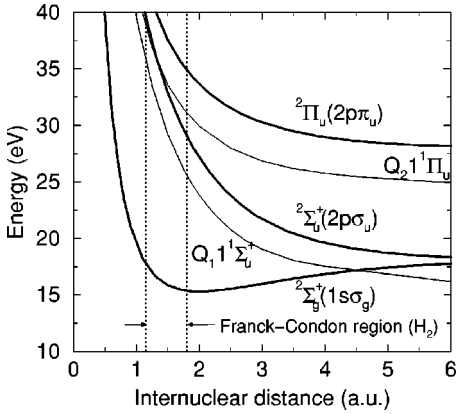

FIG. 1. Potential-energy curves of H_2 and H_2^+. The curves for autoionizing doubly excited states have been taken from Refs. [28,29]. The energy origin is placed on the lowest rovibrational level of the ground electronic state of H_2.

and nuclear wave functions. This allows one to use algebraic techniques in solving the systems of coupled equations that include the interference between the various ionization and dissociation channels. As the complete formalism was explained in detail in Ref. [21], here we only summarize the basic ingredients and adapt the notation to the multichannel case.

In the dipole approximation, the cross section for ionization from the initial state $\Psi_{g\nu}(\mathbf{r},R)$ is given by [27]

$$\sigma_{\alpha v_\alpha}(E)=\frac{4\pi^2\omega}{3c}\sum_{plm}\left|\int dR\langle\Psi_{g\nu}|\mathbf{e}_p\cdot\mathbf{D}|\Psi^+_{\alpha v_\alpha l_\alpha mE}\rangle\right|^2, \tag{1}$$

where g and ν indicate the initial electronic and vibrational states, respectively, $\hbar\omega$ is the photon energy, $\mathbf{e}_p$ is the photon polarization vector, $\mathbf{D}$ is $\mathbf{r}_1+\mathbf{r}_2$ (the length gauge), and $\Psi^+_{\alpha v_\alpha l_\alpha mE}(\mathbf{r},R)$ is the final state. In the latter state, the superscript $+$ indicates the usual outgoing boundary conditions in electron-molecule scattering; l_α and m are the angular momentum quantum numbers of the ejected electron; $E=W_{g\nu}+\hbar\omega$ with $W_{g\nu}$, the total energy of the molecule in the initial state; and α and v_α denote the electronic and vibrational states of the residual molecular ion, respectively. In this work, α stands for the $^2\Sigma_g^+(1s\sigma_g)$ and $^2\Sigma_u^+(2p\sigma_u)$ electronic states of H_2^+ or D_2^+. The label $\mathbf{r}$ is used for electronic coordinates, and R is the internuclear distance. In Eq. (1) we have factored out the rotational wave functions and averaged upon all possible orientations. The initial state is described in the framework of the Born-Oppenheimer (BO) approximation, i.e. $\Psi_{g\nu}(\mathbf{r},R)=\psi_g(\mathbf{r},R)\chi_\nu(R)$, where ψ_g is the initial electronic state and χ_ν is the nuclear vibrational wave function calculated in the potential-energy curve $E_g(R)$ associated with ψ_g:

$$[T(R)+E_g(R)-W_{g\nu}]\chi_\nu(R)=0, \tag{2}$$

where T is the relative kinetic energy of the nuclei. Here ψ_g is the $X^1\Sigma_g^+$ electronic state of H_2 or D_2, and χ_ν the vibrational state with $\nu=0$. Application of the dipole selection rules to Eq. (1) implies that only electronic states of $^1\Sigma_u^+$ and $^1\Pi_u$ symmetries are populated.

Let us call ϵ_α the kinetic energy of the outgoing electron in channel α, $\phi_r(\mathbf{r},R)$ the resonant electronic states of energy $E_r(R)$, and $\psi^{0+}_{\alpha l_\alpha m\epsilon_\alpha}(\mathbf{r},R)$ the nonresonant electronic continuum states in which the former are embedded. Then the final-state wave function can be written [20,21]

$$\Psi^+_{\alpha v_\alpha l_\alpha E}(\mathbf{r},R)=\sum_{r'}\phi_{r'}(\mathbf{r},R)\xi^{r'}_{\alpha v_\alpha l_\alpha E}(R)+\psi^{0+}_{\alpha l_\alpha\epsilon_\alpha}(\mathbf{r},R)\chi_{v_\alpha}(R)$$
$$+\lim_{\eta\to0}\sum_{r'}\sum_{\alpha' l'_{\alpha'}}\sum_{v'_{\alpha'}}\oint dE'\frac{1}{E-E'+i\eta}\int dR' V^{r'*}_{\alpha' v'_{\alpha'} l'_{\alpha'} E'}(R')\xi^{r'}_{\alpha v_\alpha l_\alpha E}(R')\psi^{0+}_{\alpha' l'_{\alpha'}\epsilon'_{\alpha'}}(\mathbf{r},R)\chi_{v'_{\alpha'}}(R), \tag{3}$$

where

$$V^r_{\alpha v_\alpha l_\alpha E}(R)=\langle\phi_r|\mathcal{H}_{\rm el}|\psi^{0+}_{\alpha l_\alpha\epsilon_\alpha}\rangle\chi_{v_\alpha}(R), \tag{4}$$

and $\mathcal{H}_{\rm el}$ is the electronic Hamiltonian. Note that we have dropped the index m because $^1\Sigma_u^+$ and $^1\Pi_u$ continuum states, which have different m's, are not coupled. In Eqs. (3) and (4), χ_{v_α} is the nuclear wave-function solution of

$$[T(R)+E_\alpha(R)-W_{v_\alpha}]\chi_{v_\alpha}(R)=0, \tag{5}$$

where $E_\alpha(R)$ is the potential-energy curve of the α state of H_2^+ or D_2^+, W_{v_α} is the energy of the residual H_2^+ or D_2^+ ion, $E=\epsilon_\alpha+W_{v_\alpha}$, and $\xi^r_{\alpha v_\alpha l_\alpha E}$ is the solution of [21,24,25]

$$[E-E_r(R)-T(R)]\xi^r_{\alpha v_\alpha l_\alpha E}(R)=V^r_{\alpha v_\alpha l_\alpha E}(R)+\lim_{\eta\to0}\sum_{r'}\sum_{\alpha' l'_{\alpha'}}\sum_{v'_{\alpha'}}\oint dE'\frac{V^r_{\alpha' v'_{\alpha'} l'_{\alpha'} E'}(R)}{E-E'+i\eta}\int dR' V^{r'*}_{\alpha' v'_{\alpha'} l'_{\alpha'} E'}(R')\xi^{r'}_{\alpha v_\alpha l_\alpha E}(R'). \tag{6}$$

The latter equation represents the nuclear motion when the electrons are in the quasistationary state ϕ_r. Equations (3) and (6) are exact within the BO approximation [21,25]. The matrix element in Eq. (4) represents the coupling between the resonance ϕ_r and the nonresonant wave function $\psi^{0+}_{\alpha l_\alpha\epsilon_\alpha}$ and vibrational state χ_{v_α}. Hence the two terms on the right-hand side of Eq. (6) are the result of the autoionizing character of the ϕ_r state. In particular, the last term represents the decay of the resonant state to the adjacent electronic continuum. This term, as well as the last one in Eq. (3), is non-

local due to the presence of the $\xi^r_{\alpha v_\alpha l_\alpha E}$ functions, and it can be split into a δ-function term and a principal value term. In applying Eqs. (3) and (6), we have excluded the bound electronic states because contributions from the latter to the ionization process is expected to be negligible.

Now some words are appropriate concerning our description of the electronic and the nuclear wave functions in Eqs. (3) and (6). The one-electron functions are defined in an interval $[0,r_{\max}]$ in terms of a basis of B-spline functions B_i^k of order k [26]. The B_i^k functions are piecewise polynomials of degree $k-1$, and are distributed along a linear knot sequence defined in the $[0,r_{\max}]$ interval. Additional knot points are defined in the borders of the interval, so that $B_i^k(0)=B_i^k(r_{\max})=0$ for all i, which is equivalent to enclosing the system in a box of size $r_{\max}$. The H_2^+ orbitals φ_{nm} are obtained by diagonalizing the H_2^+ Hamiltonian in the above basis; hence they are written

$$\varphi_{nm}=\frac{1}{r}\sum_{l=0}^{l_{\max}}\left[\sum_{i=1}^{N_l} a_i^{nl}B_i^k(r)\right]Y^{lm}(\hat{r}), \tag{7}$$

where $Y^{lm}(\hat{r})$ is a spherical harmonic, and the origin of electronic coordinates have been placed in the middle of the internuclear axis. In this work we have used $k=8$, $r_{\max}=60$ a.u., $l_{\max}=11$, and $N_l=140$ (for $l=0,\ldots,l_{\max}$). The resonant wave functions ϕ_r were obtained by diagonalizing the H_2 Hamiltonian in a basis of configurations built from the above H_2^+ orbitals [28]. In the case of the $^1\Pi_u$ symmetry, the expansion included 206 configurations ($\sigma_g\pi_u$, $\sigma_u\pi_g$, $\pi_g\delta_u$, and $\delta_g\pi_u$), in which the two lowest H_2^+ orbitals, $1s\sigma_g$ and $2p\sigma_u$, were excluded in order to ensure orthogonality with continuum states (see Ref. [29] for details, and below).

The nonresonant wave functions $\psi^{0+}_{\alpha l_\alpha \epsilon_\alpha}$ describe a bound electron in either the $1s\sigma_g$ or $2p\sigma_u$ orbitals of H_2^+, and a continuum electron with angular momentum l_α. They were evaluated using the ''L^2 close-coupling'' method [30], which allows for interchannel coupling between different partial waves and yields the correct asymptotic behavior [31]. More specifically, for each channel αl_α, we define a set of orthogonal uncoupled continuum states (UCS's)

$$\zeta^0_{\alpha l_\alpha \epsilon_\alpha}(\mathbf{r}_1,\mathbf{r}_2)=\Theta(\Phi_{\alpha l_\alpha}(\mathbf{r}_1,\hat{r}_2)\varrho_{\alpha l_\alpha \epsilon_\alpha}(r_2)), \tag{8}$$

where Θ is the symmetrization operator (we only consider singlet states), $\varrho_{\alpha l_\alpha \epsilon_\alpha}$ is the radial wave function of the continuum electron, and $\Phi_{\alpha l_\alpha}$ is the channel function, which is a state of H_2^+ combined with the angular function of the scattered electron to give the correct channel symmetry. The UCS's were built using our calculated $1s\sigma_g$ and $2p\sigma_u$ orbitals for H_2^+ and a radial continuum wave function expanded in a B-spline basis with well-defined angular momentum l_α. This procedure leads to a discrete spectrum $\{\epsilon_{\alpha l_\alpha n}\}$ and to discretized UCS wave functions $\tilde{\zeta}^0_{\alpha l_\alpha n}$ that have been renormalized using the appropriate density of states. We have evaluated all αl_α open channels with angular momentum up to $l_\alpha=7$. As in Ref. [31], interchannel coupling between the UCS's is introduced using a Lippman-Schwinger formalism

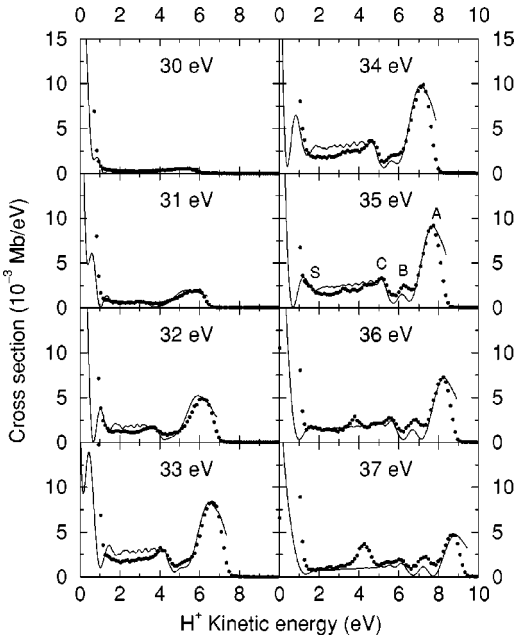

FIG. 2. KED spectra of H_2 for protons detected at 90° ($^1\Pi_u$ contribution). Solid line: theory; circles: experimental results from Ref. [17].

[30]. The corresponding Green's function is evaluated as described by Martín [32]. In previous works [28,29], we showed that this procedure provides accurate energy positions and autoionization widths for a large number of doubly excited states of H_2. In this work we only consider the lowest Q_2 $^1\Pi_u$ doubly excited state because it has the largest autoionization width of the series [29,33]. This state lies above the $^2\Sigma_u^+(2p\sigma_u)$ ionization threshold at $R\geqslant 1.35$ a.u. At shorter R, the energy curve crosses the threshold and, therefore, the state can only decay to the lowest state of H_2^+ (see Fig. 1).

The ground state of H_2 has been taken from Ref. [21] (it is represented in a basis of 400 two-electron configurations built from B-splines). Since we have used the same electronic Hamiltonian for H_2 and D_2 (infinite nuclear mass approximation), all electronic wave functions described above are identical for both systems.

The initial and final (bound and continuum) vibrational wave functions are written as linear combinations of B-spline functions B_j^k of order k;

$$\chi_\nu(R)=R^{-1}\sum_j^N d_{\nu j}B_j^k(R). \tag{9}$$

The B splines are defined in an interval $[0,R_{\max}]$ using a linear knot sequence with additional knot points in the borders so that $B_i(0)=B_i(R_{\max})=0$ for all i. Here we have used $N=240$, $k=8$, and $R_{\max}=12$ a.u. The coefficients $d_{\nu j}$ are evaluated by substituting Eq. (9) into Eqs. (2) and (5). The same B-spline basis has been used to solve Eq. (6), using the procedure described in Ref. [21].

III. RESULTS AND DISCUSSION

In Figs. 2 and 3 we show the calculated KED spectra for the $^1\Pi_u$ continuum of H_2 and D_2. The maximum allowed

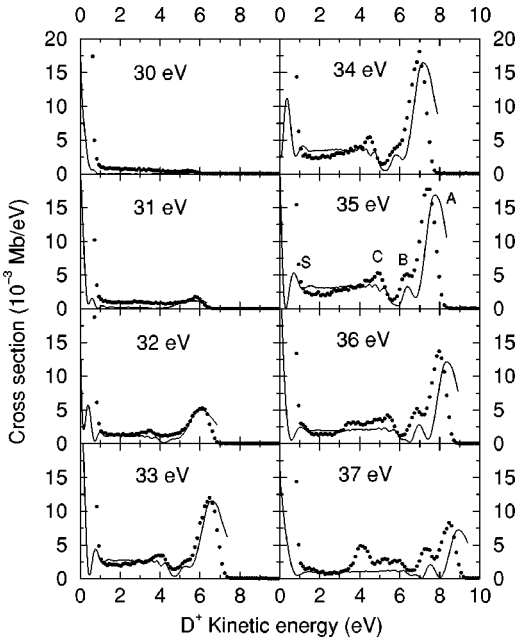

FIG. 3. KED spectra of D_2 for deuterons detected at 90° ($^1\Pi_u$ contribution). Solid line: theory; circles: experimental results from Ref. [17].

kinetic energy for ejected protons (and deuterons) is given by $T_{\max}=(\hbar\omega-E_{\rm th})/2$, where $E_{\rm th}$ is the threshold energy for dissociative photoionization ($E_{\rm th}=18.083$ eV for H_2 and 18.162 eV for D_2). Thus the theoretical cross sections must go abruptly to zero for $T=T_{\max}$ (this vertical fall is not shown in the figures for the sake of clarity). In Figs. 2 and 3 our results are compared with the spectra measured by Ito, Hall, and Ukai [17] for protons and deuterons observed at 90° with respect to the polarization vector of the incident radiation (as noted before, for this observation angle, only the $^1\Pi_u$ continuum is populated). Since the measurements are not given on an absolute scale, the experimental data have been normalized to reproduce the calculated H_2 cross section for $\hbar\omega=34$ eV and a proton kinetic energy of 7 eV. The same normalization contant is used for all photon energies and for both H_2 and D_2, so that the experimental relative intensities remain unchanged. For $\hbar\omega<36$ eV, the theory reproduces well the peaks *A*, *B*, and *C* observed in Ref. [17], as well as their relative intensities. It is then clear that the origin of all these peaks is the single doubly excited state Q_2 $1^1\Pi_u$. Although contributions from other Q_2 resonances cannot be totally excluded, it should be less important since they lie higher in energy and their autoionization widths are much smaller (e.g., the width of the second Q_2 $^1\Pi_u$ resonance is already ten times smaller at the equilibrium distance $R_e=1.4$ a.u. [29,33]). Only peak *A* is present in the experiment of Latimer *et al.* [22]; however, its intensity as a function of photon energy is also in very good agreement with the present results for both H_2 and D_2.

For $\hbar\omega\geqslant 36$, experiments [17,22] show the existence of another peak around 4 eV (this is particularly clear at 37 eV). As pointed out in Refs. [17] and [22], this peak corresponds to direct ionization to the $^2\Pi_u(2p\pi_u)$ state of H_2^+; therefore, it cannot be reproduced by the present calculations because only the two lowest ionization channels $^2\Sigma_g^+(1s\sigma_g)$ and $^2\Sigma_u^+(2p\sigma_u)$ have been included.

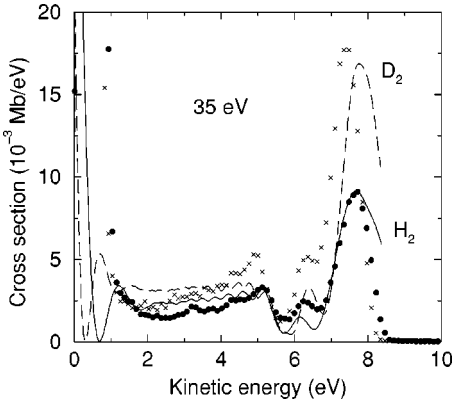

FIG. 4. Comparison between the calculated KED spectra for H_2 (solid line) and D_2 (dashed line) with the experimental ones of Ref. [17] for protons (circles) and deuterons (crosses) detected at 90° and $\hbar\omega=35$ eV.

For H_2 the positions of peaks *A*, *B*, and *C* are in good agreement with the experiment of Ref. [17]. This is also the case for D_2 up to 32 eV, but for higher photon energies the calculated positions for peak *A* are slightly shifted to higher kinetic energies. This is more clearly seen in Fig. 4, where the hydrogen and deuterium results are compared with the experimental ones at $\hbar\omega=35$ eV. The theory predicts that the position of peak *A* is roughly the same for H_2 and D_2, whereas the experiment of Ref. [17] shows that peak *A* for D_2 appears at lower kinetic energies ($\simeq 0.2$ eV) than for H_2. A similar shift is found in Ref. [17] for all photon energies above 32 eV. In contrast, the spectra of Ref. [22] do not exhibit a noticeable shift between H_2 and D_2 results, in agreement with our findings. In this respect, it must be pointed out that there is no indication that our D_2 results are less accurate than the H_2 ones because the electronic wave functions are the same for the two molecules and the nuclear wave functions have been evaluated to the same degree of accuracy. Also, the maximum allowed kinetic energy for D^+, $T_{\max}$, seems to be slightly smaller in the experiment of [17] than expected from the formula $2T_{\max}=\hbar\omega-18.162$ eV.

The partial cross sections for dissociation through the

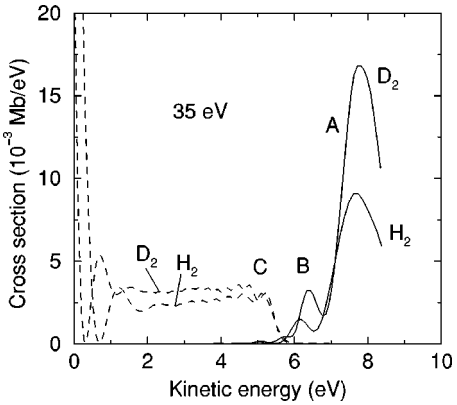

FIG. 5. Partial KED cross sections of H_2 and D_2 for protons and deuterons detected at 90° ($^1\Pi_u$ contribution) and $\hbar\omega=35$ eV. Solid lines: $^2\Sigma_u^+(2p\sigma_u)$ channel; dashed lines: $^2\Sigma_g^+(1s\sigma_g)$ channel.

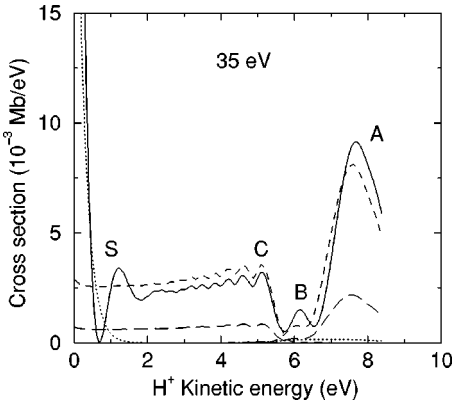

FIG. 6. Contributions to the 35-eV KED spectrum of H_2 of the different terms entering the definition of the total wave function given in Eq. (3). Solid line: total cross section; short-dashed line: resonant contribution corresponding to the first term in Eq. (3); long-dashed line: resonant contribution corresponding to the third term in Eq. (3); dotted line: nonresonant contribution corresponding to the second term in Eq. (3).

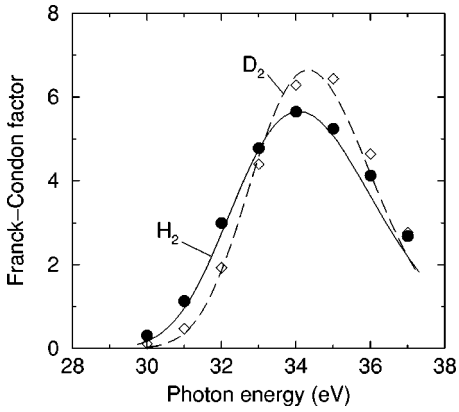

FIG. 7. Comparison between calculated Franck-Condon (FC) factors $|\langle\chi_\nu|Y_E\rangle|^2$ and calculated peak *A* intensities. Solid line: FC for H_2; dashed line: FC for D_2; circles: peak *A* intensity for H_2; diamonds: peak *A* intensity for D_2. Peak intensities have been obtained from the peak maxima in Figs. 2 and 3; they have been normalized to the FC factors at the maximum position.

$^2\Sigma_g^+(1s\sigma_g)$ and $^2\Sigma_u^+(2p\sigma_u)$ channels are shown in Fig. 5. It can be seen that they contribute in two separate regions of the spectra. The $^2\Sigma_u^+(2p\sigma_u)$ cross section leads to peaks *A* and *B* at high KE, and is practically zero at smaller KE (e.g., it is negligible below $\simeq 5$ eV in the spectrum at 35 eV). The $^2\Sigma_g^+(1s\sigma_g)$ cross section is responsible for the remaining structures and it is negligible in the region where peaks *A* and *B* appear. Figure 6 shows that peaks *A* and *B* arise from the resonant terms in the $^2\Sigma_u^+(2p\sigma_u)$ channel [first and third terms on the right-hand side of Eq. (3)]; the corresponding nonresonant background [the second term on the right-hand side of Eq. (3)] is very small and barely contributes to the spectra. Peak *C* comes from the resonant terms in the $^2\Sigma_g^+(1s\sigma_g)$ channel. The nonresonant background in the latter channel is responsible for the rapid decay of the cross section from zero to $\simeq 1.5$ eV. In this interval one can see a strong oscillation (denoted *S*) whose shape depends on photon energy. It is clear from Fig. 6 that this oscillation is the result of the interference between the resonant and nonresonant amplitudes. Although the experiments are not conclusive for kinetic energies smaller than 1.5 eV in the 30–37 photon energy range, similar oscillations have been predicted [23] and observed [17] at smaller photon energies. Peaks *A*, *B* [channel $^2\Sigma_u^+(2p\sigma_u)$] and *C* [channel $^2\Sigma_g^+(1s\sigma_g)$] can be related to autoionization of the $Q_2\ 1^1\Pi_u$ state at three different internuclear distances R_i. These can be approximately determined from the formula [17]

$$2T_i=\hbar\omega+W_{g\nu}-E_{\mathrm{H}_{1s}}-[E_r(R_i)-E_\alpha(R_i)], \qquad (10)$$

where T_i and $[E_r(R_i)-E_\alpha(R_i)]$ are the kinetic energies of the ejected proton and electron, respectively, $E_{\mathrm{H}_{1s}}$ is the ground-state energy of the H atom, and $W_{g\nu}-E_{\mathrm{H}_{1s}} \simeq 18.083$ eV ($\simeq 18.162$ for D_2). T_i is directly obtained from the position of maximum *i*. For peak *A* we obtain that R_A varies from 1.8 to 1.6 a.u. in the photon energy range 30–37 eV. This means that autoionization occurs immediately after the doubly excited state is populated. This is consistent with the fact that the corresponding partial autoionization width (see Refs. [23,29,33]) is maximum at $R=1.35$ a.u. Figure 7 shows that, for both H_2 and D_2, the cross sections at the *A* maximum position are proportional to the Franck-Condon (FC) factor $|\langle\chi_\nu|Y_E\rangle|^2$, where Y_E is the nuclear wave function that results from the equation

$$[E-E_r(R)-T(R)]Y_E(R)=0. \qquad (11)$$

The maximum intensities are obtained for $\hbar\omega=34.2$ and 34.4 eV, respectively, in good agreement with experiments. Notice that Eq. (11) can be easily solved and results from neglecting the autoionizing character of the resonance in Eq. (6). Therefore, the mechanism leading to peak *A* is very simple and can be summarized as follows: (i) the resonance is populated according to the Franck-Condon principle, (ii) the molecule begins dissociation following the repulsive potential energy curve of the $Q_2\ 1^1\Pi_u$ resonance, (iii) the resonance autoionizes at R_A, and (iv) the molecule dissociates completely following the $^2\Sigma_u^+(2p\sigma_u)$ potential-energy

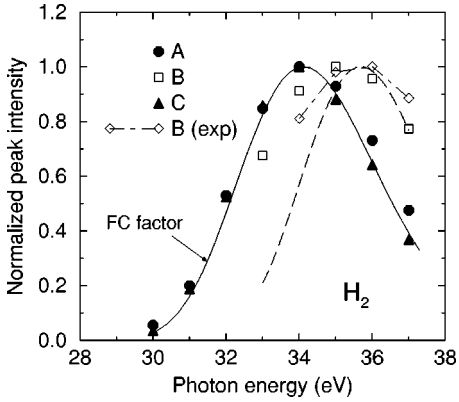

FIG. 8. Peak intensities as functions of photon energy. Circles: peak *A* (theory); squares: peak *B* (theory); triangles: peak *C* (theory); diamonds: peak *B* (experiment of Ref. [17]); solid line: Franck-Condon (FC) factor $|\langle\chi_\nu|Y_E\rangle|^2$; dashed line: $|\langle\chi_\nu|Y_E\rangle|^2|\langle\chi_{\nu_\alpha}|Y_E\rangle|^2$ (see text). Peak intensities have been obtained from the peak maxima in Figs. 2 and 3. All intensities and FC factors are normalized to 1 at the maximum position.

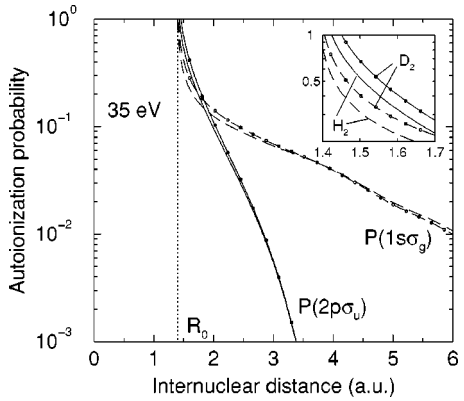

FIG. 9. Semiclassical autoionization probabilities [see Eq. (12)] as functions of internuclear distance for $\hbar\omega=35$ eV. Solid line: $^2\Sigma_u^+(2p\sigma_u)$ channel for H_2; full line with dots: $^2\Sigma_u^+(2p\sigma_u)$ channel for D_2; dashed line: $^2\Sigma_g^+(1s\sigma_g)$ channel for H_2; dashed line with dots: $^2\Sigma_g^+(1s\sigma_g)$ channel for D_2. R_0 is the classical turning point. The inset is a blow up of the short R region.

curve. Figure 8 shows that peak C exhibits a FC behavior as well; hence the mechanism is similar, except that now dissociation follows the $^2\Sigma_g^+(1s\sigma_g)$ curve in step (iv). From Eq. (10), we obtain $R_C>7$ a.u., but the existence of a near-plateau on the left side of peak C indicates that autoionization occurs in fact in the interval $[R_e,R_C]$. This is a consequence of the slow decrease of the $^2\Sigma_g^+(1s\sigma_g)$ partial width with R (see Refs. [23,29,33] and below).

We turn now to peak B. From Eq. (10), we obtain $R_B=2.7-2.6$ a.u., which is significantly larger than R_A. Furthermore, Fig. 8 shows that the intensity of peak B is not proportional to the Franck-Condon factor $|\langle\chi_\nu|Y_E\rangle|^2$. Indeed, for H_2, both theory and experiment show that the largest intensity occurs now at $\hbar\omega\simeq 35.5$ eV. To understand the origin of this unusual behavior, one has to analyze the $\xi^r_{\alpha\nu_\alpha l_\alpha E}$ function resulting from Eq. (3). Since this function combines all dissociation pathways and the interference between them, a second mechanism is possible: (i) the photon populates initially the electronic continuum associated with the $^2\Sigma_u^+(2p\sigma_u)$ state—this step is more or less independent of photon energy, because there is always maximum FC overlap; (ii) the molecule begins dissociation following the $^2\Sigma_u^+(2p\sigma_u)$ energy curve, (iii) the resonance is populated at $\simeq R_A$ due to coupling with the electronic continuum, i.e., the inverse of autoionization due to the inhomogeneous term in Eq. (6); (iv) the resonance autoionizes at R_B; and (v) the molecule dissociates completely following the $^2\Sigma_u^+(2p\sigma_u)$ energy curve. From step (iii), the probability of this second mechanism is roughly proportional to $|\langle\chi_{\nu_\alpha}|Y_E\rangle|^2$ [notice that χ_{ν_α} is the solution of Eq. (5) for $\alpha\equiv{}^2\Sigma_u^+(2p\sigma_u)$]. Since this mechanism interferes with the direct mechanism discussed above, the intensity of peak B should be proportional to $|\langle\chi_\nu|Y_E\rangle|^2|\langle\chi_{\nu_\alpha}|Y_E\rangle|^2$. This leads to the dashed curve shown in Fig. 8, which qualitatively explains the non-Franck-Condon behavior of peak B. Mechanisms involving more steps are less probable because the $^2\Sigma_u^+(2p\sigma_u)$ autoionization width is practically zero for $R>R_B$. A similar behavior is observed for peak B in D_2.

Figure 7 shows that, as expected, the Franck-Condon region is narrower for D_2 than for H_2. However, the most significant isotope effect is that the intensity of peak A is twice as large in D_2 as in H_2 (see Fig. 4). This can be partially explained by the fact that the Franck-Condon factor is larger for the former than for the latter (see Fig. 7). However, the difference is not large enough to account for a factor of 2. For this, one has to consider the autoionization probability for the Q_2 $1^1\Pi_u$ doubly excited state. Using a simple semiclassical model [34,35] in which the nuclear motion is treated classically, one can write the probability of decay into channel α as a function of R:

$$P_\alpha(R)=\frac{\Gamma_\alpha(R)}{\hbar v(R)}\exp\left[-\int_{R_0}^{R}\frac{\Gamma(R')}{\hbar v(R')}dR'\right], \qquad (12)$$

where Γ is the total autoionization width, Γ_α is the partial width for autoionization in the α channel, R_0 is the classical turning point, and v is the classical radial velocity of the nuclei moving in the E_r potential. The latter is given by

$$\tfrac{1}{2}\mu[v(R)]^2=\hbar\omega+W_{g\nu}-E_r(R), \qquad (13)$$

where μ is the reduced mass. The results obtained using this formula for $\hbar\omega=35$ eV are shown in Fig. 9. At short R, where autoionization to the $^2\Sigma_u^+(2p\sigma_u)$ is dominant, deuterium autoionization probabilities are larger than the hydrogen ones (see the inset in Fig. 9). This difference can be explained as a velocity effect: D_2 dissociates more slowly and, therefore, spends more time traversing the region of maximum autoionization than does H_2; hence the D_2 autoionization probability is enhanced. At long internuclear distances, the probabilities for both isotopes are very small in agreement with our previous findings for R_A. Thus the increase of intensity of peak A in D_2 is explained by a larger Franck-Condon factor combined with a larger autoionization probability. In the case of the $^2\Sigma_g^+(1s\sigma_g)$ channel, the latter effect is relatively less important because autoinization is not negligible at long R, where, as shown by Fig. 9, the difference between D_2 and H_2 probabilities is very small (see Fig. 9).

IV. CONCLUSION

We have presented theoretical calculations of dissociative photoionization of H_2 and D_2 in the range of photon energies 30–37 eV. The theoretical method makes use of B-spline functions to describe both electronic and nuclear wave functions. Interference among different dissociation, ionization and autoionization channels are included consistently. Partial cross sections have been computed and the different contributions have been analyzed in detail. We have shown that the resonance structures observed in the 90° KED spectra are due to autoionization of the Q_2 $1^1\Pi_u$ doubly excited state to the $^2\Sigma_g^+(1s\sigma_g)$ and $^2\Sigma_u^+(2p\sigma_u)$ states of H_2^+. At least two different mechanisms are responsible for the various peaks observed in each dissociation channel: a direct (Franck-Condon) mechanism and a multistep (non Franck-Condon) mechanism. Both of them can be easily distinguished by plotting the peak intensities as functions of photon energy. The direct mechanism leads to the most intense peak in each

dissociation channel, while the multistep mechanism leads to less intense peaks (the number of which depends on how fast the partial widths decrease at long R). This interpretation is supported by recent experimental results of Ito, Hall, and Ukai [17]. The resonance peaks for D_2 are more intense than for H_2 as a result of a more effective Franck-Condon overlap and a higher autoionization probability. The magnitude of this isotope effect is in good agreement with the measurements of Ito, Hall, and Ukai [17] and Latimer *et al.* [22].

We are grateful to Professor K. Ito for sending us the files containing the experimental data. This work was supported by the DGICYT under Project No. PB96-0056. I.S. acknowledges the Ministerio de Educación y Ciencia for a research contract.

[1] R. J. van Brunt and L. J. Kieffer, Phys. Rev. A **2**, 1293 (1970).
[2] A. Crowe and J. W. McConkey, J. Phys. B **6**, 2088 (1973); Phys. Rev. Lett. **31**, 192 (1973).
[3] J. A. Stockdale, V. E. Anderson, A. E. Carter, and L. Deleanu, J. Chem. Phys. **63**, 3886 (1975).
[4] K. Köllmann, J. Phys. B **11**, 339 (1978).
[5] J. L. Gardner and J. A. R. Samson, Phys. Rev. A **12**, 1404 (1975).
[6] A. L. Ford, K. K. Docken, and A. Dalgarno, Astrophys. J. **195**, 819 (1975).
[7] S. V. ONeil and W. P. Reinhardt, J. Chem. Phys. **69**, 2126 (1978).
[8] B. van Wingerden, Ph E. van der Leeuw, F. J. de Heer, and M. J. van der Wiel, J. Phys. B **12**, 1559 (1979).
[9] J. L. Dehmer and D. Dill, Phys. Rev. A **18**, 164 (1978).
[10] S. Strathdee and R. Browning, J. Phys. B **12**, 1789 (1979).
[11] K. Kirby, S. Guberman, and A. Dalgarno, J. Chem. Phys. **70**, 4635 (1979).
[12] K. Kirby, T. Uzer, A. C. Allison, and A. Dalgarno, J. Chem. Phys. **75**, 2820 (1981).
[13] S. Kanfer and M. Shapiro, J. Phys. B **16**, L655 (1983).
[14] M. Landau, R. I. Hall, and F. Pichou, J. Phys. B **14**, 1509 (1981); F. Pichou, R. I. Hall, M. Landau, and C. Shermann, *ibid.* **16**, 2445 (1983).
[15] K. Ito, P. Lablanquie, P. M. Guyon, and I. Nenner, Chem. Phys. Lett. **151**, 121 (1988).
[16] Y. M. Chung, E.-M. Lee, T. Masuoka, and J. A. R. Samson, J. Chem. Phys. **99**, 885 (1993).
[17] K. Ito, R. I. Hall, and M. Ukai, J. Chem. Phys. **104**, 8449 (1996).
[18] Z. X. He, J. N. Cutler, S. H. Southworth, L. R. Hughey, and J. A. R. Samson, J. Chem. Phys. **103**, 3912 (1995).
[19] C. J. Latimer, K. F. Dunn, N. Kouchi, M. A. McDonald, V. Srigengan, and J. Geddes, J. Phys. B **26**, L595 (1993); J. Geddes, K. F. Dunn, N. Kouchi, M. A. McDonald, V. Srigengan, and C. J. Latimer, *ibid.* **27**, 2961 (1994).
[20] I. Sánchez and F. Martín, Phys. Rev. Lett. **79**, 1654 (1997).
[21] I. Sánchez and F. Martín, Phys. Rev. A **57**, 1006 (1998).
[22] C. J. Latimer, J. Geddes, M. A. McDonald, N. Kouchi, and K. F. Dunn, J. Phys. B **29**, 6113 (1996).
[23] I. Sánchez and F. Martín, Phys. Rev. Lett. **82**, 3775 (1999).
[24] J. N. Bardsley, J. Phys. B **1**, 349 (1968).
[25] A. U. Hazi, T. N. Rescigno, and M. Kurilla, Phys. Rev. A **23**, 1089 (1981).
[26] C. de Boor, *A Practical Guide to Splines* (Springer, New York, 1978).
[27] I. Cacelli, V. Carravetta, A. Rizzo, and R. Moccia, Phys. Rep. **205**, 283 (1991).
[28] I. Sánchez and F. Martín, J. Chem. Phys. **106**, 7720 (1997).
[29] I. Sánchez and F. Martín, J. Chem. Phys. **110**, 6702 (1999).
[30] M. Cortés and F. Martín, J. Phys. B **27**, 5741 (1994).
[31] I. Sánchez and F. Martín, J. Phys. B **30**, 679 (1997).
[32] F. Martín, Phys. Rev. A **48**, 331 (1993).
[33] J. Tennyson, At. Data **64**, 253 (1996).
[34] W. H. Miller, J. Chem. Phys. **52**, 3563 (1970).
[35] A. U. Hazi, J. Chem. Phys. **60**, 4358 (1974).